Combustion and Flame 268 (2024) 113623

Contents lists available at ScienceDirect

Combustion and Flame

journal homepage: www.sciencedirect.com/journal/combustion-and-flame

Spray flame characterisation under lean blow-out conditions

Fabian Hampp [a,b,*], Dominik Schäfer [b], Oliver Lammel [b]

[a] Institute of Combustion Technology for Aerospace Engineering, University of Stuttgart, Pfaffenwaldring 38-40, Stuttgart, 70569, Germany
[b] Institute of Combustion Technology, German Aerospace Center (DLR), Pfaffenwaldring 38-40, Stuttgart, 70569, Germany

ARTICLE INFO

Keywords:
Lean blow-out approach
Damköhler scaling
Spray combustion
Dual airblast injector
Liquid fuel MGT

ABSTRACT

The scalability of liquid fuel operated jet stabilised combustion systems towards dimensions and mixing timescales relevant for compact designs (e.g. MGT, compact aero-engines) is impeded by the lack of suitable injection concepts. The high momentum of the combustion air jet can deteriorate the spray quality of conventional injection systems leading to elevated emissions rendering prompt primary atomization essential. For this purpose, a canonical confined jet spray burner was recently developed and equipped with a novel in-house dual pressure swirl/airblast injection concept. In the current study, the lean blow-out (LBO) sensitivity, a critical design parameter of aero-engines, of the spray burner is delineated across an extensive parameter variation on the jet bulk velocity ($80 \leq u_j(\mathrm{m/s}) \leq 160$), combustion air preheat temperature ($500 \leq T_j(\mathrm{K}) \leq 800$), premixing length ($0.0 \leq l_m(\mathrm{mm}) \leq 48$) and fuel type (Jet-A1, extra light heating oil and n-dodecane) with distinctly different distillation curves. The spray and combustion process of a partially premixed and direct injection hardware configurations are characterised by means of phase Doppler interferometry (PDI) and OH^*-chemiluminescence imaging during the LBO approach, i.e. equivalence ratio (Φ) reduction. N-dodecane exhibits highest resilience against LBO, followed by Jet-A1 and finally heating oil. The PDI results show that atomization and physical fuel properties, i.e. viscosity, are not the driving cause for the measured LBO sensitivity. To delineate the observed LBO fuel sensitivity, the data analysis is further supported by a leading order Damköhler number scaling to determine progress limiting processes, e.g. vaporisation, mixture formation and auto-ignition based reaction onset. The enhanced auto-ignition propensity of n-dodecane in comparison to the complex fuels leads to differences in the measured flame lift-off height as well as the spatial heat release distribution and fluctuation during the LBO approach. However, the chemical Damköhler numbers (flame and auto-ignition) do not support the measured difference in LBO sensitivity between the complex fuels Jet-A1 and Oil. By contrast, the determined vaporisation timescales align with the measured LBO fuel ranking, suggesting that mixture formation is strongly influenced by the vaporisation process and resulting reactivity stratification assumes a dominant role in LBO sensitivity.

Novelty and significance

The current work delineates the lean blow-out (LBO) sensitivity in compact liquid fuel operated high momentum jet stabilised combustion systems over a wide operation condition and physical fuel properties. The present study extends the combustor design critical parameter of LBO to such burner concepts with a targeted application in future lean premixed hybrid aero-engines. For this purpose, a canonical single nozzle confined jet spray burner with an in-house dual pressure swirl/airblast injector was recently develop. The excellent atomization performance of the utilised injection system allows an investigation of the LBO sensitivity independent from the atomizer performance and thereby separating physical (namely viscosity and atomization) from fuel chemistry effects. The consistent mixture quality offers further novel insights on the thermochemical conversion process during the LBO approach highlighting the significance of vaporisation in the LBO process itself and of auto-ignition in the combustion process near LBO.

1. Introduction

The global aviation sector contributes approximately 5% to the anthropogenic climate change [1] of which non-CO_2 emissions account

* Corresponding author at: Institute of Combustion Technology for Aerospace Engineering, University of Stuttgart, Pfaffenwaldring 38-40, Stuttgart, 70569, Germany.
E-mail address: fabian.hampp@ivlr.uni-stuttgart.de (F. Hampp).

https://doi.org/10.1016/j.combustflame.2024.113623
Received 5 May 2024; Received in revised form 12 July 2024; Accepted 14 July 2024
Available online 24 July 2024

for 50–75% [2]. The latter consists of predominantly nitrogen oxide (NO_X), particulates and water vapour that promote the formation of contrail cirrus's [3]. While the use of carbon-neutral fuels can mitigate CO_2, the reduction of particulates and NO_X is strongly dependent on the fuel composition as well as the involved thermophysical and -chemical processes. In this context, lean premixed combustion technologies are highly attractive to minimise NO_X and particulates of future aero-engine including hybrid concepts [4]. Homogeneous mixing is key to effectively reduce (thermal) NO_X and particulates by mitigating local peak temperatures and fuel rich regions and the atomization performance is critical in this context [5]. The use of carbon-neutral aviation fuels will also create a diverse market that necessitates fuel flexible injection systems and combustion processes.

In terms of fuel flexibility of the combustion process, high momentum jet stabilised combustion systems are well suited for operation from 100% H_2 to extra light heating oil, while offering low emissions [6,7]. The associated burning modes work best under homogeneously premixed conditions. This inherently puts stringent requirements on the injection of liquid fuels that can be relaxed by long mixing timescales or wet combustion [6,7]. However, in compact FLOX combustor designs, e.g. for future application in hybrid aero-engines, such methods are not feasible, rendering atomization performance the decisive criterion to fully capitalise on the benefits of the associated burning mode. The recently developed dual injection system [8] uses a pressure swirl (PS) injector for prefilming onto an airblast wall. Such injection concepts provide excellent operational flexibility and are frequently used in gas turbine swirl burners, e.g. aero-engines [9,10]. The work by Lefebvre et al. [11,12] showed good fuel flexibility of airblast concepts for hydrocarbon fuels with viscosities similar to kerosene. By contrast, the fuel placement (e.g. spray angle) and atomization of pressure swirl injectors are sensitive to a comparable physical fuel properties variation [13]. Moreover, the high momentum air flow can exhibit adverse effects on droplet size and fuel placement [14,15] For combustion applications with high air preheat temperatures, the liquid fuel viscosity is more affected by the preheating process rather than the chemical composition of various conventional and synthetic fuels e.g. [16]. To this end, airblast injection remains a promising concept to cope with a fuel diverse market.

Lean blow-out (LBO), besides instabilities, remains one of the major concerns of lean premixed combustion systems [17] and is a critical aero-engine design parameter [18]. Blow-out, i.e. global extinction, occurs when the chemical timescale (flame or auto-ignition) becomes longer than the residence time. In general, the chemical flame timescale increases with decreasing equivalence ratio [19], reaction onset temperature [20] and fuel reactivity [21] as well as increasing inert gas dilution [22]. Under premixed conditions LBO is kinetically controlled while non-premixed spray systems are inherently influenced by atomization, mixing and vaporisation and may limit LBO [23]. Esclapez et al. [24] investigated the effect of fuel reactivity on LBO and found that corresponding empirical correlations cannot capture fuel chemistry effects. The driving source of uncertainty and LBO sensitivity was attributed to droplet size and multi-component evaporation. A common conclusion is that mixture inhomogeneities [25], e.g. due to non-ideal atomization and less volatile fuels, enhance LBO performance. The competing effects of physical and chemical fuel properties are strongly air preheat temperature dependent [23], where conditions below the flash point lead to a vaporisation limited LBO rendering the physical fuel properties decisive. By contrast, for high preheat temperatures, the fuel chemistry, namely auto-ignition propensity or derived cetane number, provided the strongest LBO correlation. The effect of mixture homogeneity was described by Cavaliere et al. [26] by delineating LBO characteristics under premixed, non-premixed and spray combustion. When determining Damköhler numbers (Da) of the latter two configurations at stoichiometric conditions, all three flames extinguished at the same critical Da enabling the use of timescale correlations to delineate LBO performance. The presence of predominantly small droplets (<80 μm) render gas phase interactions (i.e. reaction progress) dominant in the combustion process and can improve LBO performance due to the stabilisation of a lifted partially premixed flame in a swirl stabilised burner [18]. The aforementioned have focused on swirl flames, while Windom and co-workers [27–29] utilised an annular co-flow spray burner to delineate LBO behaviour of jet fuels. In addition to mixture inhomogeneities that arise from reduced vaporisation rates or larger droplets, the heat of combustion was identified as additional LBO influencing parameter. To our knowledge, LBO of high momentum jet stabilised spray flame burners has not been investigated in detail, in particular considering a potential deteriorating spray quality in the LBO approach due to changes in the atomizer performance.

The overarching object of the current research is the utilisation of liquid fuels in auto-ignition influenced low NO_X combustion processes moving towards lean premixed combustion with an intended use case for future hybrid aero-engine concepts or MGT systems for decentralised heat and power solutions. For this purpose, we evaluate the lean blow-out characteristics over a broad range of operating conditions (i.e. bulk jet velocity (u_j), air preheat temperature (T_j) and injection system recess length) and fuels (Jet-A1, extra light heating oil and n-dodecane) in a recently developed confined jet single nozzle spray burner (CJSB) with an in-house dual injection system [8]. The atomizer performance facilitates the separation of physical (atomization and vaporisation) and chemical processes (flame propagation or auto-ignition) processes. In the following, the experimental and diagnostic setup are described in Section 2, while the LBO approach strategy and data analysis is detailed in Section 3. The results are subsequently discussed in Section 4 with the work concluded in Section 5.

2. Experimental and diagnostic setup

The utilised single nozzle confined jet spray burner, the dual injector as well as the diagnostic setup are briefly introduced below with a more detailed description provided by Hampp et al. [8].

2.1. Burner facility

A single nozzle confined jet spray burner (CJSB), schematically depicted in Fig. 1 with a more detailed description provided by Hampp et al. [8], consists of three main parts: (i) a burner body providing the combustion air, (ii) an optical accessible combustion chamber (i.e. rectangular cross section of $40 \times 50\,mm^2$, length of 600 mm) and (iii) a liquid fuel injection system. The combustion air is supplied by a calibrated Bronkhorst mass flow controller (inflow series) to the burner. Multiple deflections and a porous plate decouple the air from inflow effects and provide an axisymmetric flow field to the injection system. Subsequently, the combustor nozzle is converging to its final inner diameter of D = 12 mm. The cylindrical nozzle section is at least 72 mm long ($6D$) and can be extended by additional $6D$ using spacer elements. The combustor nozzle is placed 10 mm off-centred in the based plate of the combustion chamber to create a pronounced recirculation zone. This simulates the flow and flame stabilisation conditions of the corresponding full burner design that consist of multiple circular arranged nozzles creating an inner recirculation zone. A PID controlled electric inline heater (Leister LE 10 000 DF-R) can supply the combustion air at a temperature of up to 800 K. A nitrogen pressurised piston cylinder supplies the liquid fuel fluctuation-free to the burner facility. The centralised (within the combustor nozzle) fuel supply lance consists of three coaxially joined tubes, where the inner duct supplies the liquid fuel, the middle supplies the cooling water and the outer one returns it. This offers fuel temperature control to around 315 K at the injector tip, measured via a thermocouple, independent of operation conditions.

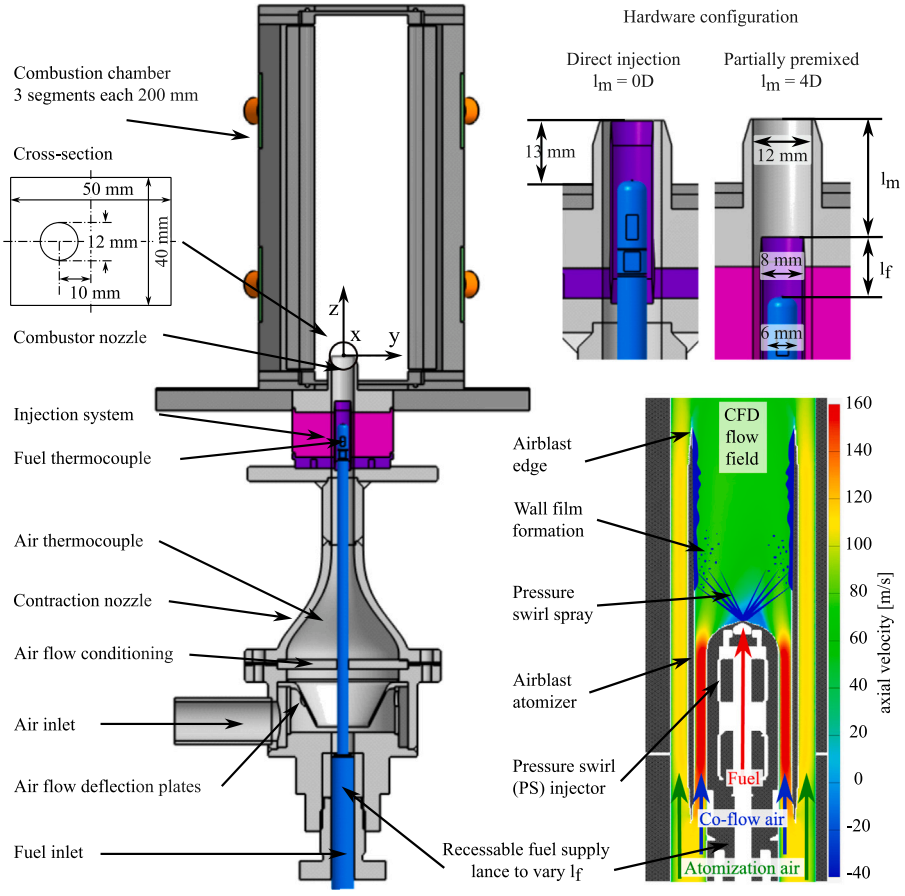

Fig. 1. Schematic of the developed single nozzle confined jet spray burner and the developed dual pressure swirl/airblast injection concepts with the main components labelled. The coordinate system is also defined with the origin fixed at the centre of the combustor nozzle exit. The CFD-based flow field of the pure axial air flow to evaluate the geometric air split for the case u_j = 120 m/s is also shown by means of the false colour background on the right hand side including colour scale. Note that the mixing length (l_m) and film length (l_f) are not shown to scale.

2.2. Injection concept

A major challenge of liquid fuel operated jet stabilised GT combustors is the injection system scalability towards compact designs, while achieving the required flexibility and low emissions. For this purpose, a novel dual injection system was developed [8] that combines a custom pressure swirl (PS) injector (nominal flow number FN0.25, mass flow rate: 0.20 - 0.70 g/s) with an airblast concept, see bottom right of Fig. 1. For academic purposes, the complete geometry of the injection system can be made available upon request. The PS injector creates a hollow cone spray with a nominal spray angle of 90° and forms a film on the inner airblast wall. The position of the airblast wall creates a geometric air split into atomization (outer) and co-flow (inner) air. The axial PS injector position is stepless adjustable creating the film length (l_f), while the axial distance between the airblast and combustor nozzle edge can be altered by means of spacer elements from 0D to 6D in steps of 0.5D, here named mixing length (l_m). In the current study, the film length is fixed to 8.0 mm (i.e. one inner diameter of the wall film duct), while l_m is varied between 0D and 4D, defining the direct injection (DI) and partially premixed (PM) hardware configurations, respectively.

2.3. Diagnostic setup

Phase Doppler interferometry (PDI) is used to quantify the atomization performance with the spray symmetry assured via shadowgraphy (not included). The combustion process is analysed using OH*-chemiluminescence (CL) images. A diagnostic system schematic [8] is provided in SMM Fig. S1.

An Artium Technologies Inc. three-phase Doppler interferometry system (Model PDI-300 MD) is used to measure the droplet size distribution and velocity with focus on the former. Due to the optical access into the rectangular combustion chamber, the PDI receiver collects signal at a 74° forward scattering configuration. The transmission and receiver optics exhibit a focal length of 350 mm. The receiver aperture slit width is set to 250 µm determining the spatial resolution. The hardware and software settings feature droplet size measurements from 0.8 to 120 µm.

OH*-chemiluminescence marks the heat release zone [30,31] and provides insights into the flame shape, lift-off and penetration. The OH*-CL signal is recorded with an intensified camera unit (LaVision sCMOS) and intensifier relay optics (IRO) that is equipped with a Halle UV lens (focal length of 64 mm) and a narrow bandpass filter from AHF (peak transmission of 85%, fhw of 310 ± 15 nm). The IRO settings are maintained constant at a gain of 85% and a gate time of 80 µs to facilitate case comparison. The resulting field of view is 61.7 × 200 mm^2 with an optical resolution of 0.8 mm, determined with an USAF 1951 resolution target.

2.4. Operation conditions

In the general CJSB characterisation [8], a reference case was defined with an air jet bulk velocity (u_j) of 120 m/s, an air preheat temperature (T_j) of 650 K, an equivalence ratio (Φ) of 0.80 and an injector recession or mixing length (l_m) into the combustor nozzle of 4D (i.e. 48.0 mm). To delineate LBO performance of the dual injector system and auto-ignition influenced spray flame, the fuel mass flow rate

Table 1
Overview of all cases investigated, where T_j is the air jet preheat temperature and u_j the air jet bulk velocity. The Reynolds number is determined on bulk properties (i.e. $Re = u_j \cdot D/\nu_j$). The Weber number (We), conventional Damköhler number (Da_c) at a stoichiometry of Φ = 0.60 (i.e. a value close to LBO) and vaporisation Da are determined using Eq. (1) for the partially premixed injector hardware configuration $l_m = 4D$. For the DI cases, the We numbers are approximately twice as high, while the Da_c is 30 ± 2% lower. The vaporisation Damk^{f}ohler number (Da_v) values for the DI cases are, on average also 25% lower, yet the variance is distinctly stronger in comparison to the systematic difference for We and Da_c. Values for the DI cases are provided in the SMM Table S2.

Case	Fuel	u_j	T_j	Re	We	Da_c	Da_v
–	–	m/s	K	$\times 10^3$	$\times 10^{-2}$	–	–
1a	Jet	80	650	54.5	3.39	1.45	0.30
1b	Oil	80	650	54.3	3.34	1.28	0.27
1c	nDod	80	650	54.6	2.19	1.62	0.32
2a	Jet	120	650	81.7	3.31	1.09	0.47
2b	Oil	120	650	81.5	3.67	0.96	0.43
2c	nDod	120	650	81.9	2.76	1.22	0.50
3a	Jet	160	650	109	7.78	0.79	0.59
3b	Oil	160	650	109	4.83	0.69	0.48
3c	nDod	160	650	109	3.59	0.88	0.56
4a	Jet	120	500	75.2	4.20	0.41	0.40
4b	Oil	120	500	76.0	5.04	0.36	0.36
4c	nDod	120	500	75.4	3.71	0.47	0.42
5a	Jet	120	800	87.6	2.26	2.49	0.56
5b	Oil	120	800	87.4	2.74	2.23	0.50
5c	nDod	120	800	87.7	2.02	2.76	0.60

Table 2
Overview of selected fuel properties. The density, kinematic viscosity and surface tension are inferred at 293 K.

Property	Unit	Jet	Oil	nDod
Density	kg/m^3	813	838	750
kin. viscosity	mm^2/s	~2.0	4.4	1.8
Surface tension	N/m	0.023	0.024	0.027
LHV	MJ/kg	43.2	42.8	44.1
dest. start	K	427	444	490
dest. 50%	K	477	570	490
dest. end	K	542	632	490
Aromatic content	%	18.0	28.6	0.0

is gradually reduced while maintaining all other parameters constant. LBO is investigated for different jet bulk velocities ($80 \leq u_j$ (m/s) ≤ 160), air preheat temperatures ($500 \leq T_j$ (K) ≤ 800), mixing lengths ($0D \leq l_m$ (mm) $\leq 4D$) and fuel types (Jet-A1, extra light heating oil (Oil), n-dodecane (nDod)) with a summary of all conditions provided in Table 1.

An overview of selected fuel properties is presented in Table 2 with surrogates composition included in the supplementary material and methods (SMM Table S1). The used Oil has distinctly higher kinematic viscosity (ν = 4.4 mm^2/s) and distillation curve end ($\delta_{v,1}$ = 632 K) in comparison to Jet-A1 (ν = 2.0 mm^2/s, $\delta_{v,1}$ = 542 K) and n-dodecane (ν = 1.8 mm^2/s, $\delta_{v,1}$ = 490 K). Moreover, Oil is composed of nearly 29% aromatic content.

3. Methodology

3.1. Lean blow-out approach

Lean blow-out is approached by gradually reducing the fuel mass flow rate and thus Φ. This approach is consistent and beneficial for the comparison with numerical studies [24] as the gaseous inflow, i.e. u_j and T_j, are not affected. In the present configuration, the ignition and flame stabilisation is strongly influenced by the recirculation zone and entrained hot combustion products [6,32–35]. Thus, in order to conduct a repeatable LBO experiment, the following procedure is applied:

1. Ignite at given u_j and T_j at $\Phi \simeq 0.80$.
2. Reduce equivalence ratio at constant u_j and T_j to $0.05 \leq \Phi - \Phi_{\mathrm{LBO}}$ (–) ≤ 0.10.
3. Thermally equilibrate the combustor.
4. Gradually reduce Φ at a rate $\sim 1 \cdot 10^{-3}$ s^{-1} to $\Phi = \Phi_{\mathrm{LBO}} + 0.02$ by injection pressure reduction.
5. Reduce Φ at a rate $\sim 2 \cdot 10^{-4}$ s^{-1} until LBO.
6. Record Φ at LBO and repeat at least 3 times.

The temperature reduction due to heat-up and vaporisation of the liquid fuel is between 25 to 50 K for the entire operation condition variation and predominantly dependent on the liquid fuel mass flow rate. Fuel differences in the latent heat of evaporation or liquid heat capacity lead to estimated variations below 5 K for the three fuels.

3.2. Data analysis

During LBO approach, the injection pressure is gradually reduced. This can affect the performance of the pressure swirl atomizer used for pre-filming on the airblast edge, in particular as the fuel mass flow rate is at the lower design range of the injector. In order to evaluate the spray quality effect on LBO characteristics, radial profiles of the droplet size distribution are measured at different heights (i.e. z = 2.0, 12.0 - only for DI, and 48.0 mm) at $\Phi = \Phi_{\mathrm{LBO}} + 0.01$. The PDI sample size consists of more than 10,000 data points with probe volume correction conducted in AIMS v7.3 [36]. The latter accounts for the droplet size dependent detection volume bias [7].

For each operating condition, 500 instantaneous OH*-CL images ($I_{i,\mathrm{OH^*}}$) are recorded with a frame rate of 40 Hz. The flame lift-off height and extinction point are delineated via image binarisation ($B_{i,\mathrm{OH^*}}$), utilising an instantaneous background method [8]. Moreover, proper orthogonal decomposition (POD) is conducted on the image intensity fluctuation (i.e. $I'_{\mathrm{OH^*}} = I_{i,\mathrm{OH^*}} - \overline{I_{\mathrm{OH^*}}}$). Subsequently, the energy distribution of the POD modes is determined. A broad distribution is indicative of a strong spatially fluctuating OH*-CL signal that is attributed to turbulent transport of the heat release zone. By contrast, a narrow mode distribution represents a stable flame.

3.3. Non-dimensional numbers

3.3.1. Turbulent flow

The turbulent Reynolds number (Re_t) is defined in Eq. (1), where L_I is the integral length scale. The definition of a unique L_I-value is ambiguous in a developing turbulent jet. In order to provide comparable Re_t and also Damköhler numbers, a minimum integral length scale is estimated. In turbulent free shear flows, $L_I = c \cdot \delta_j$ in a downstream region of $x/L_{ref} > 15$, where δ_j is the jet spread width, L_{ref} the nozzle diameter or width of the obstructing element and c = 0.4 and 0.8 for planar jets and grid obstructed flows, respectively [37]. In the current setup, the combustor nozzle diameter with D = 12.0 mm creates the first reference value, while the central PS injector with OD of 6.0 mm creates the second one based on obstructed flow. Assuming no jet spread, i.e. $L_{ref} = \delta_j$, provides the lower limit and both approaches provide the same value of L_I = 4.8 mm. The inherent jet spread or a position closer to the nozzle exit yield higher values. The root mean squared velocity fluctuations (u') are determined based on the droplet velocity. The use of droplets as gaseous flow tracers represents a conservative estimation of u' as the Stokes numbers are above unity. Given that the measured droplet sizes are not strongly fuel property dependent, this leads to a consistent underestimation of Re_t and integral timescale ($\tau_I = L_I/u'$) and the validity of the intended comparison across the different fuel cases remains. The kinematic viscosity (ν) of the preheated air temperature (T_j) and fuel mixture is determined assuming complete evaporation.

3.3.2. Atomization and vaporisation

The Weber number (We), defined in Eq. (1), is determined based on the Sauter mean diameter (SMD, d_{32}) and u', measured at (x, y, z) = (0.0, 0.0, 2.0) and (0.0, 0.0, 12.0) mm for the partially premixed and direct injection cases, respectively. The air jet density (ρ_j) is determined at T_j and the fuel surface tension (σ) at the fuel injection temperature (T_l = 315 K). Vaporisation timescales are estimated following the methodology of Abramzon and Sirignano [38] considering forced convection and physical fuel properties as function of temperature [39], while applying a rapid mixing limit to within droplet. The droplet heating and vaporisation process is calculated with an initial time step of 1 μs that is adjusted to limit the incremental surface temperature increase from 0.01–1.0 K. In order to evaluate the validity of the rapid mixing limit assumption, a conduction limit model, i.e. the lower limit, is calculated simultaneously with thermal equilibrium reached within the time step. The initial droplet diameter and temperature are set to the measured d_{32} and injection temperature (T_l = 315 K) at the nozzle exit, the ambient temperature is set to T_j and heat and mass transfer coefficients are determined based on the measured velocity fluctuations. The distillation curves are approximated by a linear regression ($R^2 > 0.97$). While this is arguably rather crude, it allows to adjust latent heat during a sequential evaporation process using the relation provided by Kistiakowsky [40]. The vaporisation model is validated against the experimental data of Stöhr et al. [41] with good agreement in terms of heat-up phase, droplet swelling (or the absence of it for Jet-A1) and vaporisation timescales (τ_v). Moreover, the effect of sequential evaporation leading to the intersection of the n-dodecane and Jet-A1 diameter reduction ($t/D_0^2 \simeq 3.7$ vs. 4.0) is captured with reasonable accuracy in the current 0D model. Thus, for the present leading order analysis, the implemented models is capable of separating physical fuel property and operation condition effects. The axial velocity decay [42] and hot gas entrainment rate [43] of the turbulent jet are estimated along the symmetry axis to include the present recirculation zone to simulate the associated increase in ambient temperature during the vaporisation process. This leads to a conservative estimate of the vaporisation timescales as radial transport is omitted and droplets away from the symmetry axis are exposed to higher ambient temperatures and therefore evaporate faster. The liquid fuel temperature is measured within the PS injector tip and the heat transfer to the fuel during film formation and forced convection is neglected. To evaluate the sensitivity, T_l is increased by 100 K leading to a systematic reduction of the vaporisation timescales by 12 ± 2%. In order to evaluate the vaporisation process influence on the mixture formation, a corresponding Damköhler number (Da_v) is defined in Eq. (1) based on the integral flow and the complete droplet vaporisation timescale including the heat-up period. This is in contrast to the definition by Verwey and Birouk [44,45], who defined Da_v based on the flow field around a droplet and a steady state vaporisation rate and Won et al. [46], who demonstrated that a partial vaporisation model improves LBO sensitivity towards fuel properties in a liquid swirl burner. In the present work, turbulence enhancing effects of the vaporisation rate have been readily considered in the model determining τ_v. Given the measured droplet sizes, dispersion is dominated by turbulent transport and the provided Da_v values relate vaporisation to turbulent mixing. As discussed below, the provided conservative estimate suggests that vaporisation is completed prior to droplet interaction with the reaction zone rendering the assumption valid.

3.3.3. Reaction chemistry

The chemical timescales (τ_c and τ_{ai}) and corresponding conventional (Da_c) and auto-ignition-based Damköhler number (Da_{ai}) [47], see Eq. (1), are determined based on detailed chemistry calculations. The former is inferred from the thermal laminar flame thickness to flame speed ratio using the DLR concise reaction mechanism [48] in Cantera. The auto-ignition delay time calculations are conducted using the Polimi reaction mechanism to include low temperature chemistry [49,50]. For Oil and Jet-A1, surrogates are created [51] based on GCxGC analysis with the composition provided in the SMM Table S1. In the current configuration, the reaction onset temperature increases with exhaust gas recirculation rate (ζ). This is simulated by means of a reactor network, where the equilibrated combustion products are mixed adiabatically with the reactants from ζ = 0.0 to 1.0 in steps of 5% followed by a stirred reactor calculation to determine the ignition delay time. This approach approximates the temperature rise in the current configuration and considers exhaust gas dilution effects in the auto-ignition based reaction onset.

$$Re_t = \frac{L_I \cdot u'}{\nu_j}\ ; \qquad We = \frac{\rho_j \cdot u'^2 \cdot d_{32}}{\sigma}$$

$$Da_v = \frac{\tau_I}{\tau_v}\ ; \qquad Da_c = \frac{\tau_I}{\tau_c}\ ; \qquad Da_{ai} = \frac{\tau_I}{\tau_{ai}} \tag{1}$$

4. Results

In the following, the effects influencing LBO (i.e. atomization, vaporisation and fuel chemistry) are separated to identify the leading cause. OH*-CL images and flame photographs are depicted in Fig. 2 for the partially premixed Jet-A1 flame for the extreme operation conditions to provide a visual impression of the flame shape and position as well as the effect of operation condition on the combustion process. The flame with Φ = 0.60 is close to the LBO point (Φ_{LBO} = 0.55) and the spatially distributed heat release zone deep into the recirculation zone is evident. Moreover, the low intensity jet core with a penetration depth of up 150 mm highlights the delayed reaction zone. The illustrated trend is qualitatively representative for all fuels with differences emerging under very lean conditions approaching LBO as discussed below.

4.1. Lean blow-out

The LBO performance for the different fuel types (Jet-A1, Oil and n-dodecane), bulk jet velocities ($80 \leq u_j$ (m/s) ≤ 160), air preheat temperatures ($500 \leq T_j$ (K) ≤ 800) and mixing lengths is depicted in Fig. 3. All fuels show a very similar trend with respect to u_j and T_j, yet systematic differences are apparent. Although differences are subtle, there is a clear fuel separation trend. With respect to Jet-A1, n-dodecane exhibits an improved LBO performance by $\Delta\Phi_{\mathrm{LBO}} = -0.02$ and vice versa for Oil with $\Delta\Phi_{\mathrm{LBO}} = 0.02$ over the entire u_j and T_j variation. The experimental repeatability in determining Φ_{LBO} is 0.007. In general, mixture stratification enhances LBO performance for all fuels consistently with the DI cases leading to a lower $\Delta\Phi_{\mathrm{LBO}}$ of 0.02 in comparison to the partially premixed (here denoted as PM) cases. This is in line with literature as discussed above. By contrast, with increasing bulk flow velocity, the LBO performance increases by approximately 5%–10% despite improved atomization as delineated below. Spatially distributed vaporisation due to higher convective transport of droplets can lead, in combination with reduced mixing timescales, to elevated mixture inhomogeneities. Moreover, with increasing u_j, the recirculation zone strengthens and the shorter residence time leads to reduced relative heat loss [32]. Both augment auto-ignition due to enhanced entrainment of a higher enthalpy EGR state [19]. The LBO sensitivity as a function of air preheat temperature is distinctly stronger, i.e. ≈ 30% when increasing T_j from 500 to 800 K. As atomization is not affected by the T_j-variation, this can be attributed to predominantly two effects. First, an increase in T_j results in an elevated reaction onset temperature, reduced chemical timescales for given Φ and, in turn, a higher temperature of recirculated exhaust gas. Second, with increasing T_j, the fuel mass flow is reduced due to the constant u_j and vaporisation is enhanced e.g. [23]. The latter causes an initial temperature reduction of $\Delta T_{vap} \simeq 30$ and 60 K at T_j = 500 and 800 K, respectively, that is similar for all fuels for a given operation condition.

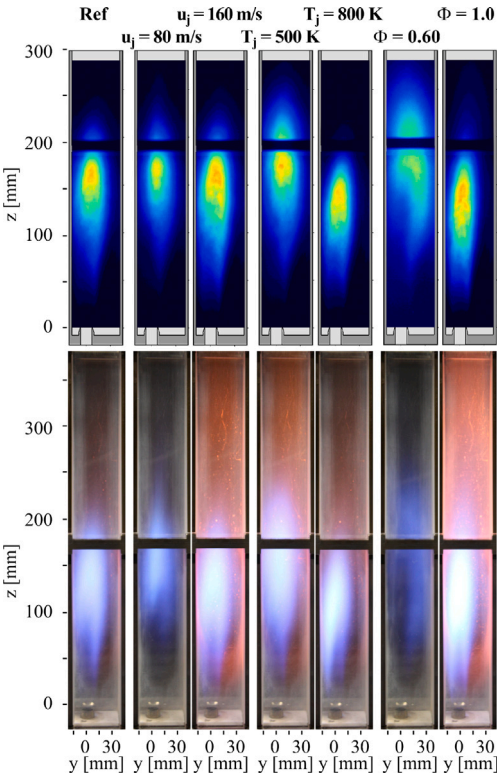

Fig. 2. OH*-CL images and flame photographs for partially premixed Jet-A1 flames for the extreme operation conditions. The case marked by Ref. refers to the conditions u_j = 120 m/s, T_j = 650 K, Φ = 0.80. All other cases are varied away from the reference case. The flame with Φ = 0.60 is close to the LBO point (Φ_{LBO} = 0.55) for this condition. The absence of soot is evident even at globally stoichiometric conditions.

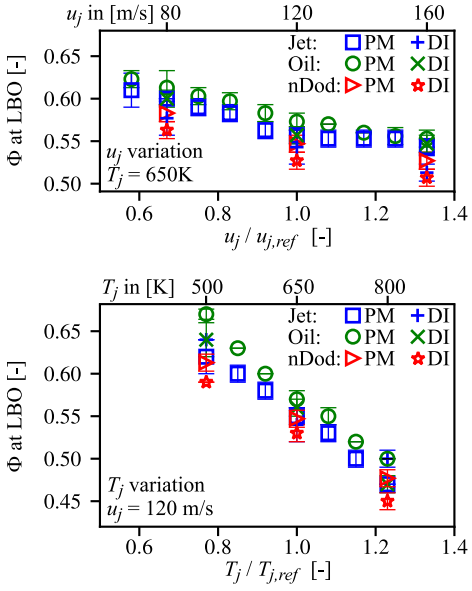

Fig. 3. Equivalence ratio at LBO (Φ_{LBO}) as a function of normalised initial temperature ($T_j/T_{j,ref}$, bottom panel) and bulk velocity ($u_j/u_{j,ref}$, top panel), where the index *ref* refers to the reference condition T_j = 650 K and u_j = 120 m/s. The marker shows the mean and the bars the standard deviation from a minimum of three experiments.

4.2. Atomizer performance approaching LBO

First, the change in droplet size distribution during LBO approach is evaluated for the cases declared in Table 1, and depicted in Fig. 4

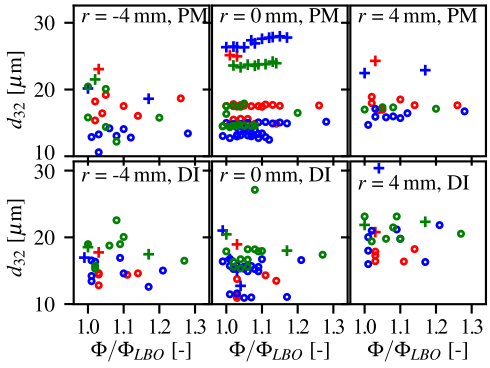

Fig. 4. Scatter plot showing the injection pressure and thus mass flow rate effect on d_{32} during the LBO approach over Φ, normalised by Φ at LBO, at three radial positions, i.e. in the centre at r = 0.0 mm and above the airblast edge at r = ±4.0 mm. The top (bottom) row shows the PM (DI) cases and the colour coding is consistent with Fig. 3, i.e. blue — Jet-A1, green — Oil, red — nDod. The + -symbols identify the u_j = 80 m/s and the ∘-symbols all other cases.

at three different radial positions, i.e. on the centreline and at r = ±4.0 mm above the airblast edge. Full radial profiles at Φ_{LBO} are shown in the SMM Fig. S2. It is worth noting, that the d_{10} diameters show very similar trends. On the abscissa, Φ is normalised by the case-dependent Φ_{LBO}. The partially premixed cases (top row) are measured at z = 2.0 mm (closest measurement location to the injector) and the direct injection cases are determined at z = 12.0 mm (a position where primary break-up is completed). As shown, the scatter of measured d_{32} enhances in the LBO approach, yet no systematic droplet size increase is observed when reducing fuel mass flow rate. Moreover, the physical fuel properties (in particular viscosity) do not exhibit a noticeable effect on the atomizer performance, suggesting that primary atomization is dominated by the aerodynamic forces acting on the airblast edge. In general, the d_{32} is not strongly affected by the operation conditions with the exception of the PM u_j = 80 m/s case. Nonetheless, the latter yields $d_{32} \leq$ 30 μm, with constant sizes during LBO approach. The mean SMD of all cases in Fig. 4 is 17.2 ± 3.9 μm and 15.9 ± 2.6 μm when excluding the u_j = 80 m/s cases. This corresponds to a modest d_{32} variation of 23% and 16% during the LBO approach, respectively, over a wide range of fuel mass flow rates (i.e. $\dot{m}_l$ = 0.19 and 0.50 g/s). Consequently, atomization and a deteriorating spray quality is not the driving cause for the observed LBO differences with respect to operation conditions and physical fuel properties.

4.3. Vaporisation

The calculated vaporisation process of characteristic droplets is depicted for all PM cases in Fig. 5. The initial conditions are based on the measured data, i.e. d_{32} and u' at (x, y, z) = (0.0, 0.0, 2.0), T_l = 315 K, $T_{inf,0} = T_j$, initial droplet velocity $u_{d,0} = u_j$ and fuel properties as defined in Table 2. The left panels of Fig. 5 depict the temporal evolution of d^2 with both axes scaled by the initial diameter ($d_0^2 = d_{32}^2$), while the right panels show d as function of time. Four, arguably non-surprising, observations are made: (i) the evaporation time scale is dominated by the initial droplet diameter, e.g. see the case u_j = 80 m/s for all fuels, (ii) the upper end of the distillation curve dictates the fuel ranking of the determined vaporisation timescales, (iii) high (low) preheat conditions result in an early (late) onset of the droplet mass loss due to phase change and (iv) high turbulent intensities amplify vapour convection and enhance evaporation rates. The first point also emphasises the importance of excellent primary atomization for liquid fuel operated high momentum jet stabilised combustion systems, that perform best in fully premixed conditions.

Values of the vaporisation Damköhler number are provided for the partially premixed cases in Table 1 ranging from 0.27 ≤ Da_v (–)

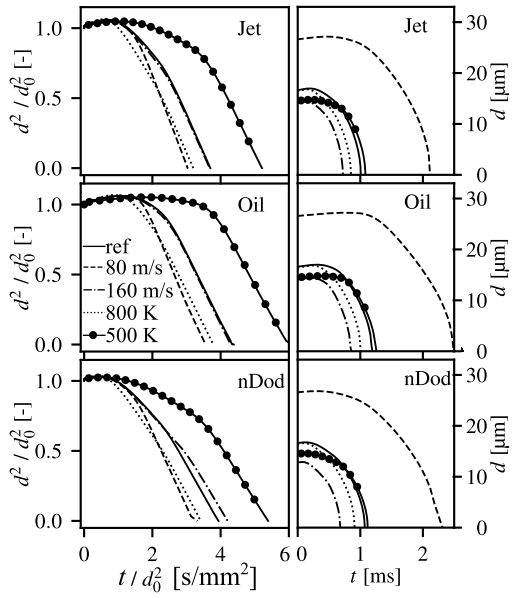

Fig. 5. Droplet vaporisation process using the experimental initial conditions (i.e. $d_0 = d_{32}$ at the nozzle exit, T_0, u_j, T_j), fuel properties (see Table 2) and assumptions on jet spread and exhaust gas entrainment. The left column depicts the d^2/d_0^2 reduction and the right column d as function of time for Jet-A1 (top row), Oil (middle row) and n-dodecane (bottom row). The five different line style depict the five different operation conditions.

≤ 0.60. Values below unity indicate that the mixture formation and homogenisation rate is strongly influenced by the vaporisation process. By contrast, high values of Da_v indicate that phase change is concluded within one integral timescale of turbulence. With this and the upper distillation curve ends of the three fuels in mind, see Table 2 and for all cases SMM Table S2, it is not surprising that Oil exhibits the lowest and nDod the highest Da_v values with Jet-A1 situated in between. This effect is strongest under conditions of high heat transfer rates to droplets and high vapour convection rates, i.e. T_j = 800 K and u_j = 160 m/s. The determined Da_v further suggest that the vaporisation process is concluded within four integral timescales and can be considered reasonably fast, in particular as droplets away from the symmetry axis are exposed to higher ambient temperatures and turbulent strain, both promoting vaporisation. With respect to bulk flow timescales and flame lift-off height measurements (see below), data suggest that the vaporisation process is completed prior to interaction with the reaction zone. The absence of soot related to individual droplet burning supports this interpretation. At the same time, the Da_v values indicate the role of sequential evaporation during the mixture formation process. Won et al. [46] reported an improved LBO — fuel chemistry correlation when determining the derived cetane number based on the lower distillation curve end. However, the LBO fuel ranking measured here suggests that the upper distillation curve end, i.e. large hydrocarbons with low volatility yet high auto-ignition propensity at intermediate temperatures [52,53], dictates LBO as the combustion processes is increasingly dominated by entrainment of hot combustion products promoting auto-ignition during the approach. This, and the delayed reaction onset that can accommodate complete evaporation, support the present Da_v definition based on the bulk vaporisation timescale for the intended purpose.

4.4. Fuel chemistry

In order to evaluate the fuel chemistry effects, complete evaporation and perfect premixing prior to reaction onset is assumed. While this is a coarse representation of the mixture, it allows to delineate the

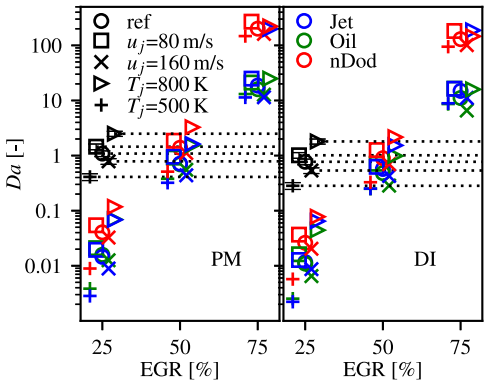

Fig. 6. Effect of fuel chemistry and operation conditions on Da_c and Da_{ai} at LBO. Da_c is depicted as average of the three fuels by the dotted line (independent of EGR-rate) with the marker identifying the operation conditions. Da_{ai} is shown by the coloured markers at an EGR-rate of 25, 50 and 75%. The left (right) panel shows the PM (DI) cases.

fuel chemistry effects in this limit. In addition to the above analysis on vaporisation timescales, the interim formation of soot, i.e. an indicator for mixture inhomogeneities, was absent even at globally rich conditions [8], both supporting the validity of the assumption. In this context, the conventional and auto-ignition based Da are determined and depicted in Fig. 6. As the chemical timescale calculations of the PM and DI cases rely on the same assumptions, differences in Da_c and Da_{ai} stem from subtle deviations in the determined integral flow timescales. The fuel chemistry effect on Da_c is very modest and only operation condition dependent differences are depicted by the dotted lines. Inherently, the biggest differences arise from the T_j variation with Da_c increasing from 0.42 to 1.2 for 500 ≤ T_j (K) ≤ 800. The auto-ignition based Da_{ai} with adiabatic exhaust gas admixture of 50% yields very similar values. With increasing EGR rate the fuels clearly separate with Da_{ai} for n-dodecane being an order of magnitude higher than for Jet-A1 and Oil. The exception is the case Jet-A1, T_j = 800 K with a very similar auto-ignition delay time as n-dodecane. In general, reduced quantities of EGR admixture are required to initiate an auto-ignition based reaction onset of n-dodecane in comparison to the two complex fuel mixtures. Yet, there is no systematic difference in Da_{ai} between Jet-A1 and Oil that can lead to the LBO separation observed in Fig. 3.

4.5. Combustion during LBO approach

While the above analysis can provide guidance, the fuel chemistry effects are yet to be determined experimentally. Hampp et al. [8] have shown, by means of radially resolved flame lift-off height (l_{loh}) measurements, that the Oil flame anchoring transitions from above the nozzle exit (−6.0 < y (mm) < 6.0) and shear layer (0.0 < y (mm) < 12.0) into the recirculation zone (18.0 < y (mm) < 30.0) with decreasing Φ. LBO was previously not reached. In Fig. 7 each data point represents the mean and standard deviation of all u_j and T_j conditions for a given fuel and Φ/Φ_{LBO}. It is evident that in a PM mode, l_{loh} increases for all fuels axially above the nozzle (top row) during LBO approach, yet remains first constant and then reduces in the recirculation zone (bottom row). Under stable flame conditions (i.e. $\Phi/\Phi_{\mathrm{LBO}} \geq 1.3$) with turbulent flame propagation, fuel differences are very subtle and directly linked to Da_c (see Table 1 and SMM Table S2). For leaner conditions auto-ignition increasingly influences the flame stabilisation and n-dodecane yields an advanced flame anchoring with lower l_{loh} in line with reduced auto-ignition timescales as discussed below. Mixture stratification amplifies this effect with the nDod cases trailing off distinctly in the DI mode when approaching LBO. By contrast, the l_{loh} of Jet-A1 and Oil increases consistently and at similar rates. Yet, the transition of the lowest l_{loh} from above the

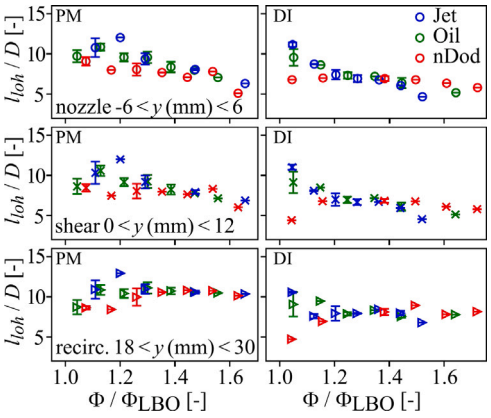

Fig. 7. Flame lift-off height in different characteristic regions during Φ_{LBO} approach. The markers and bars represent the average and standard deviation of all PM (left) or DI cases (right) of a given fuel.

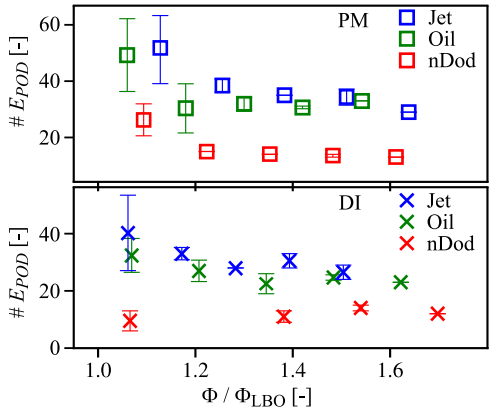

Fig. 8. Number of modes containing 80% of the POD energy while approach Φ_{LBO}. The markers and bars represent the average and standard deviation of all PM (top) or DI (bottom panel) cases of a given fuel.

nozzle into the recirculation zone remains. It is worth noting here that the reaction onset, marked by l_{loh}, is delayed enough to accommodate complete evaporation of most droplets close to LBO conditions.

The energy distribution across the POD modes (# E_{POD}) provides further insights into the spatial fluctuation of the signal intensity and is evaluated while approaching LBO for the different fuels and operation conditions (i.e. u_j, T_j and l_m) as shown in Fig. 8. As in Fig. 7, one data point is comprised of all u_j and T_j conditions for a given Φ/Φ_{LBO}. The complex fuel mixtures Jet-A1 and Oil lead to a strong broadening across multiple POD modes during the LBO approach. That is, in a stable flame 80% of the modal energy is distributed across ~30 modes, while just prior to Φ_{LBO}, the same energy is distributed across ~50 modes. The relative increase for nDod is similar ($15 \leq$ # E_{POD} (modes) ≤ 28), yet in absolute terms its flame is significantly more stable. The # E_{POD} broadening during the LBO approach is in line with the findings by Yin et al. [54] for fully premixed methane jet flames. The driving cause for LBO was identified as the entrainment of reactants and thereby reduced transport of hot combustion products into the recirculation zone. This yields local extinction, strong reignition and recovery events, i.e. spatially distributed flame puffing, that was also qualitatively observed during LBO of lean H_2 flames by Petry et al. [55] and further analysed via LES by Noh and Navarro-Martinez [56]. Phenomenologically, the LBO process of the jet stabilised spray flames investigated here is, despite the distinctly different flow field, comparable to the swirl flames investigated by Rock et al. [57]. In a recent study, Rock et al. [58] have highlighted similarities of the physical processes leading to LBO when comparing gaseous and liquid fuel operated swirl combustors. The flame shape and position resemblance during the LBO approach of fully premixed CH_4 [54] and H_2 [55] confined jet flames and the present liquid fuel operated burner underlines the role of predominant flow features driving LBO. In the future, this facilitates LBO-related Damköhler scaling as performed by Ciardiello et al. [17] for swirl-stabilised combustors. Moreover, the resilience of fuels with elevated auto-ignition propensity towards LBO appears also transferable between jet stabilised flames investigated here and swirl stabilised combustors [57]. Given that differences in the droplet size distribution and liquid loading are marginal for the different fuels and that vaporisation of Jet-A1 and Oil is significantly different, the # E_{POD} broadening is attributed by exclusion to the difference in auto-ignition delay time. The high Da_{ai} of nDod at EGR rates $\geq$ 50% yield a prompt reaction onset and turbulent transport is not sufficient to spatially distribute the reacting gas. Vice versa, for Jet-A1 and Oil the auto-ignition delay time is approximately an order of magnitude longer facilitating transport of reactants into the recirculation zone leading to the observed # E_{POD} broadening. In the DI configuration, the POD mode energy is contained in 2/3rd of number of modes in comparison to the PM cases and consistent with the previously observed l_{loh} fluctuation reduction [8]. In addition, differences between the complex fuel mixtures and nDod are stronger pronounced, while the broadening of # E_{POD} during the LBO approach is generally dampened. This is particularly prominent for the n-dodecane cases, where # E_{POD} containing 80% of the energy is limited to ~ten. The inherent elevated mixture stratification in the DI cases amplifies the occurrence of reacting gas being transported through the recirculation zone back into the shear layer, anchoring the flame. This is readily apparent at $\Phi \gg \Phi_{LBO}$, where l_{loh} differences in the defined characteristic regions are subtle, see Fig. 7. Thus, the PM cases show a stronger ignition/burning mode transition in comparison to DI during LBO approach. Yet, mixture stratification prolongs LBO to globally leaner conditions as also observed in swirl [26] and co-annular spray flames [27].

5. Discussion and conclusions

In this study, the LBO sensitivity of a high momentum jet stabilised spray flame is investigated for a wide range of operation conditions (u_j, T_j, l_m) and fuel type (Jet-A1, Oil and n-dodecane). The effects of atomization, vaporisation and combustion chemistry are separated with the support of a leading order Damköhler number scaling. With increasing u_j (T_j) the LBO performance increases modestly (distinctly). Mixture stratification (direct injection versus partially premixed) also enhances LBO performance, while nDod offers the leanest operation, followed by Jet-A1 and then Oil. These effects are subtle yet clearly separable. The atomization performance of the recently developed dual pressure swirl — airblast injector is quantified by means of droplet sizing during the LBO approach. Neither the fuel nor the operation condition variation lead to distinct differences in the measured d_{32} with values predominantly below 25 µm. Consequently, atomization is excluded as the driving cause for the measured LBO sensitivity. Fuel chemistry effects are delineated via conventional and auto-ignition Damköhler numbers in a limit analysis, where Da_c is inherently influenced by T_j, yet not strongly by the fuel type. By contrast, nDod exhibits a distinctly higher Da_{ai} in comparison to Jet-A1 and Oil with very similar values. These fuel differences are also observed in the flame lift-off height measurements and POD analysis, where the auto-ignition propensity of nDod leads to reduced l_{loh} close to LBO and a heat release zone that is less influenced by turbulent transport. The similarities in measured d_{32} and combustion performance of Jet-A1 and Oil suggest that the mixture formation process exhibits a leading influence on measured LBO differences. This is supported by the determined vaporisation Damköhler numbers that indicate delayed

completion of the sequential vaporisation process affecting mixture homogenisation for the complex fuels cases, in particular for Oil. The upper distillation curve ends of Jet-A1, Oil and nDod are 542, 632 and 490 K, respectively, and thus in line with the fuel LBO performance. Consequently, the experimental data supported by the leading order Damköhler number analysis offer a delineation of the rate-limiting processes for the underlying cause leading to LBO. A direct *Da*-scaling describing LBO in confined jet stabilised combustion systems is highly warranted, yet subject for future work. In the current burner, the LBO fuel sensitivity is arguably strongly influenced by vaporisation with the combustion process close to LBO being dominated by the fuel auto-ignition propensity. The open injector geometry renders the data an excellent foundation for developing and validating numerical models targeting the complex interaction of atomization, vaporisation and flame extinction.

CRediT authorship contribution statement

Fabian Hampp: Writing – review & editing, Writing – original draft, Visualization, Software, Methodology, Investigation, Funding acquisition, Formal analysis, Data curation, Conceptualization. **Dominik Schäfer:** Investigation, Data curation. **Oliver Lammel:** Project administration, Funding acquisition.

Declaration of competing interest

The authors declare that they have no known competing financial interests or personal relationships that could have appeared to influence the work reported in this paper.

Acknowledgements

Fabian Hampp gratefully acknowledges the funding by the German Aerospace Center (DLR), Programmdirektion Energie, FL2 Flüssig FLOX, Deutsche Forschungsgemeinschaft (DFG) - project number: 456687251. In addition, the authors thank Dr. Trupti Kathrotia for creating the surrogate mixtures used for the chemical calculations and Mr. Yeonse Kang for providing the setup schematics.

Appendix A. Supplementary data

Supplementary material related to this article can be found online at https://doi.org/10.1016/j.combustflame.2024.113623.

References

[1] V. Grewe, A.G. Rao, T. Grönstedt, C. Xisto, F. Linke, J. Melkert, J. Middel, B. Ohlenforst, S. Blakey, S. Christie, S. Matthes, K. Dahlmann, Evaluating the climate impact of aviation emission scenarios towards the Paris agreement including COVID-19 effects, Nature Commun. 12 (2021) 3841.
[2] M. Niklaß, V. Grewe, V. Gollnick, K. Dahlmann, Concept of climate-charged airspaces: a potential policy instrument forinternalizing aviation's climate impact of non-CO_2 effects, Clim. Policy 21 (2021) 1066–1085.
[3] B. Kärcher, Formation and radiative forcing of contrail cirrus, Nature Commun. 9 (2018) 1824.
[4] J.C. Gladin, C. Perullo, J.C. Tai, D.N. Mavris, A parametric study of hybrid electric gas turbine propulsion as a function of aircraft size class and technology level, in: 55th AIAA Aerospace Sciences Meeting, 2017, AIAA 2017–0338.
[5] P. Domingo-Alvarez, P. Bénard, V. Moureau, G. Lartigue, F. Grisch, Impact of spray droplet distribution on the performances of a kerosene lean/premixed injector, Flow Turbul. Combust. 104 (2020) 421–450.
[6] O. Lammel, M. Severin, H. Ax, R. Lückerath, A. Tomasello, Y. Emmi, B. Noll, M. Aigner, L. Panek, High momentum jet flames at elevated pressure, A: Experimental and numerical investigation for different fuels, in: Proc. ASME Turbo Expo, 2017, pp. GT2017–64615.
[7] F. Hampp, J.D. Gounder, H. Ax, R. Lückerath, O. Lammel, M. Hase, B. Janus, High momentum jet flames at elevated pressure, E: Quantification of droplet size distribution and transport, in: Proc. ASME Turbo Expo, 2020, pp. GT2020–14619.
[8] F. Hampp, D. Schäfer, O. Lammel, Spray flame characterisation of a dual injector for compact combustion systems, Combust. Sci. Technol. (2023) 1–34, http://dx.doi.org/10.1080/00102202.2023.2249222.
[9] G. Chaussonnet, S. Gepperth, S. Holz, R. Koch, H.J. Bauer, Influence of the ambient pressure on the liquid accumulation and on the primary spray in prefilming airblast atomization, Int. J. Multiph. Flow 125 (2020) 103229.
[10] I.A. Ibrahim, A.M. Elzallat, M.M. Elsakka, T.M. Farag, H.M. Gad, Numerical study of kerosene spray and combustion characteristics using an air-blast atomizer, Energy Rep. 8 (2022) 5974–5986.
[11] G.E. Lorenzetto, A.H. Lefebvre, Measurements of drop size on a plain jet airblast atomizer, AIAA J. 15 (1977) 1006–1010.
[12] A.A. Rizkalla, A.H. Lefebvre, The influence of air and liquid properties on airblast atomization, J. Fluids Eng. 97 (1975) 316–320.
[13] R.A. Dafsari, H.J. Lee, J. Han, J. Lee, Evaluation of the atomization characteristics of aviation fuels with different viscosities using a pressure swirl atomizer, Int. J. Heat Mass Transfer 145 (2019) 118704.
[14] N. Petry, D. Schäfer, O. Lammel, F. Hampp, Quantification of coflow effects on primary atomization of pressure swirl atomizers, Int. J. Multiph. Flow 149 (2022) 103946.
[15] B. Jose, F. Hampp, Machine learning based spray process quantification, Int. J. Multiph. Flow 172 (2024) 104702.
[16] A. Urbán, M. Malý, V. Józsa, A. Jedelský, Effect of liquid preheating on high-velocity airblast atomization: From water to crude rapeseed oil, Exp. Therm. Fluid Sci. 102 (2019) 137–151.
[17] R. Ciardiello, R.S. Pathania, I.E. Helou, E. Mastorakos, Lean blow-off investigation in a linear multi-burner combustor operated in premixed and non-premixed modes, Appl. Energy Combust. Sci. 9 (2022) 100041.
[18] G. Muthuselvan, M.S. Rao, V.S. Iyengar, M. Pulumathi, S. Thirumalachari, K. Srinivasan, Effect of atomization quality on lean blow-out limits and acoustic oscillations in a swirl stabilized burner, Combust. Sci. Technol. 192 (2019) 1028–1052.
[19] F. Hampp, R.P. Lindstedt, Strain distribution on material surfaces during combustion regime transitions, Proc. Combust. Inst. 36 (2017) 1911–1918.
[20] F. Hampp, S. Shariatmadar, R.P. Lindstedt, Quantification of low Damköhler number turbulent premixed flames, Proc. Combust. Inst. 37 (2019) 2373–2381.
[21] F. Hampp, R.P. Lindstedt, Quantification of fuel chemistry effects on burning modes in turbulent premixed flames, Combust. Flame 218 (2020) 134–149.
[22] F. Hampp, K.H.H. Goh, R.P. Lindstedt, The reactivity of hydrogen enriched turbulent flames, Process Saf. Environ. 143 (2020) 66–75.
[23] N. Rock, I. Chterev, B. Emerson, S.H. Won, J. Seitzman, T. Lieuwen, Liquid fuel property effects on lean blowout in an aircraft relevant combustor, J. Eng. Gas Turbines Power 141 (2019) 071005.
[24] L. Esclapez, P.C. Ma, E. Mayhew, R. Xu, S. Stouffer, T. Lee, H. Wang, M. Ihme, Fuel effects on lean blow-out in a realistic gas turbine combustors, Combust. Flame 181 (2017) 82–99.
[25] J. Grohmann, B. Rauch, T. Kathrotia, W. Meier, M. Aigner, Influence of single-component fuels on gas-turbine model combustor lean blowout, J. Propuls. Power 34 (2018) 97–107.
[26] D.E. Cavaliere, J. Kariuki, E. Mastorakos, A comparison of the blow-off behaviour of swirl-stabilized premixed, non-premixed and spray flames, Flow Turbul. Combust. 91 (2013) 347–372.
[27] R.A. Alsulami, B. Windell, S. Nates, W. Wang, S.H. Won, B. Windom, Investigating the role of atomization on flame stability of liquid fuels in an annular spray burner, Fuel 265 (2020) 116945.
[28] R.A. Alsulami, B.C. Windom, Liquid jet fuel property impacts on combustion performance, J. Propuls. Power 37 (2021) 276–282.
[29] R.A. Alsulami, M. Sharma, B. Windell, B. Windom, Experimental study on the effect of liquid loading on n-heptane spray jet flame stability, Exp. Therm. Fluid Sci. 147 (2023) 110953.
[30] Y. Hardalupas, C.S. Panoutsos, A.M.K.P. Taylor, Spatial resolution of a chemiluminescence sensor for local heat-release rate and equivalence ratio measurements in a model gas turbine combustor, Exp. Fluids 49 (2010) 883–909.
[31] C.S. Panoutsos, Y. Hardalupas, A.M.K.P. Taylor, Numerical evaluation of equivalence ratio measurement using OH* and CH* chemiluminescence in premixed and non-premixed methane–air flames, Combust. Flame 156 (2009) 273–291.
[32] O. Lammel, M. Stöhr, P. Kutne, C. Dem, W. Meier, M. Aigner, Experimental analysis of confined jet flames by laser measurement techniques, J. Eng. Gas Turbines. Power 134 (2012) 041506.
[33] O. Lammel, T. Rödiger, M. Stöhr, H. Ax, P. Kutne, M. Severin, P. Griebel, M. Aigner, Investigation of flame stabilization in a high-pressure multi-jet combustor by laser measurement techniques, in: Proc. ASME Turbo Expo, 2014, pp. GT2014–26376.
[34] M. Severin, O. Lammel, H. Ax, R. Lückerath, M. Aigner, High momentum jet flames at elevated pressure, B: Detailed investigation of flame stabilization with simultaneous PIV and OH LIF, in: Proc. ASME Turbo Expo, 2017, pp. GT2017–64556.
[35] M. Severin, O. Lammel, W. Meier, Laser diagnostic investigation of a confined premixed turbulent jet flame stabilized by recirculation, Combust. Flame 243 (2022) 112061.
[36] P.A. Strakey, D.G. Talley, S.V. Sankar, W.D. Bachalo, Phase-Doppler interferometry with probe-to-droplet size ratios less than unity. II. Application of the technique, Appl. Opt. 39 (2000) 3887–3893.
[37] G. Cafiero, M. Obligado, J.C. Vassilicos, Length scales in turbulent free shear flows, J. Turbul. 21 (2020) 243–257.

[38] B. Abramzon, W. Sirignano, Droplet vaporization model for spray combustion calculations, Int. J. Heat Mass Transfer 32 (1989) 1605–1618.
[39] A.H. Lefebvre, V.G. McDonell, Atomization and sprays, second ed., CRC Press, 2017.
[40] W. Kistiakowsky, Über verdampfungswärme und einige gleichungen, welche die eigenschaften der unassoziierten flüssigkeiten bestimmen, Z. Phys. Chem. 107 (1923) 65–73.
[41] M. Stöhr, S. Ruoff, B. Rauch, W. Meier, P. Le Clercq, Droplet vaporization for conventional and alternative jet fuels at realistic temperature conditions: Systematic measurements and numerical modeling, Proc. Combust. Inst. 38 (2021) 3269–3276.
[42] G. Xu, R.A. Antonia, Effect of different initial conditions on a turbulent round free jet, Exp. Fluids 33 (2002) 677–683.
[43] F.P. Ricou, D.B. Spalding, Measurements of entrainment by axisymmetrical turbulent jets, J. Fluid Mech. 11 (1961) 21–32.
[44] C. Verwey, M. Birouk, Experimental investigation of the effect of droplet size on the vaporization process in ambient turbulence, Combust. Flame 182 (2017) 288–297.
[45] C. Verwey, M. Birouk, Fuel vaporization: Effect of droplet size and turbulence at elevated temperature and pressure, Combust. Flame 189 (2018) 33–48.
[46] S. Won, N. Rock, S.J. Lim, S. Nates, D. Carpenter, B. Emerson, T. Lieuwen, T. Edwards, F.L. Dryer, Preferential vaporization impacts on lean blow-out of liquid fueled combustors, Combust. Flame 205 (2019) 295–304.
[47] F. Hampp, R.P. Lindstedt, Quantification of combustion regime transitions in premixed turbulent DME flames, Combust. Flame 182 (2017) 248–268.
[48] T. Kathrotia, P. Oßwald, C. Naumann, S. Richter, M. Köhler, Combustion kinetics of alternative jet fuels, Part-II: Reaction model for fuel surrogate, Fuel 302 (2020) 120736.
[49] G. Bagheri, E. Ranzi, M. Pelucchi, A. Parente, A. Frassoldati, T. Faravelli, Comprehensive kinetic study of combustion technologies for low environmental impact: MILD and OXY-fuel combustion of methane, Combust. Flame 212 (2020) 142–155.
[50] E. Ranzi, C. Cavallotti, A. Cuoci, A. Frassoldati, M. Pelucchi, T. Faravelli, New reaction classes in the kinetic modeling of low temperature oxidation of n-alkanes, Combust. Flame 162 (2015) 1679–1691.
[51] T. Kathrotia, P. Oßwald, C. Naumann, S. Richter, M. Köhler, Combustion kinetics of alternative jet fuels, Part-III: Fuel modeling and surrogate strategy, Fuel 302 (2020) 120737.
[52] R. Minetti, M. Ribaucour, M. Carlier, L.R. Sochet, Autoignition delays of a series of linear and branched chain alkanes in the intermediate range of temperature, Combust. Sci. Technol. 113 (1996) 179–192.
[53] M.D. Boot, M. Tian, E.J.M. Hensen, S.M. Sarathy, Impact of fuel molecular structure on auto-ignition behavior – Design rules for future high performance gasolines, Prog. Energy Combust. Sci. 60 (2017) 1–25.
[54] Z. Yin, I. Boxx, W. Meier, Influence of self-sustained jet oscillation on a confined turbulent flame near lean blow-out, Proc. Combust. Inst. 36 (2017) 3773–3781.
[55] N. Petry, M. Mannazhi, Z. Yin, O. Lammel, K.P. Geigle, A. Huber, Investigation of fuel and load flexibility of an atmospheric single nozzle jet-stabilized FLOX combustor with hydrogen/methane-air mixtures, in: Proc. ASME Turbo Expo, 2023, pp. GT2023–102392.
[56] D. Noh, S. Navarro-Martinez, Investigation of the jet-flame interaction by large EddySimulation and proper decomposition method, Combust. Sci. Technol. 191 (2019) 956–978.
[57] N. Rock, B. Emerson, J. Seitzman, T. Lieuwen, Near-lean blowoff dynamics in a liquid fueled combustor, Combust. Flame 212 (2020) 53–66.
[58] N. Rock, S. Stouffer, T. Hendershott, E. Corporan, P. Wrzesinski, The role of hydrodynamic instabilities on near-lean blowout flame shapes in a swirl-stabilized spray combustor, J. Eng. Gas Turbines. Power 145 (2023) 051013.